A Low-Power-Extended-Linear-Range Magnetic Levitator

by

Rayal St. Patrick Johnson

S.B., Massachusetts Institute of Technology (2004)

Submitted to the Department of Electrical Engineering and Computer Science
in partial fulfillment of the requirements for the degree of

Master of Engineering in Electrical Engineering

at the

MASSACHUSETTS INSTITUTE OF TECHNOLOGY

February 2007

Author .....
Department of Electrical Engineering and Computer Science
February 2, 2007

Certified by .....
Professor James K. Roberge
Professor of Electrical Engineering
Thesis Supervisor

Accepted by .....
Arthur C. Smith
Chairman, Department Committee on Graduate Students

A Low-Power-Extended-Linear-Range Magnetic Levitator

by

Rayal St. Patrick Johnson

Submitted to the Department of Electrical Engineering and Computer Science
on February 2, 2007, in partial fulfillment of the
requirements for the degree of
Master of Engineering in Electrical Engineering

Abstract

In this thesis, I designed and built analog circuits to extend the linear range of a magnetic levitator. Analog Devices AD633 multipliers are used to implement nonlinear terms which compensate for the electromagnet and sensor nonlinearities, which were measured experimentally. Implementing the nonlinear compensation allows the system to be operating point independent. Frequency compensation was done with a lead network since the resulting linearized levitator is essentially a double integrator. Position sensing was done using an OPB732 reflective switch. Nonlinear compensation for the sensor is done with an AD532 multiplier configured as a divider.

Thesis Supervisor: Professor James K. Roberge
Title: Professor of Electrical Engineering

Acknowledgments

I would like to thank Prof. James Roberge for agreeing to supervise my thesis, and guiding me through to the end. Everything is common sense to him, but not always to me, so I thank him also for having patience. Hopefully I can someday become as he. I would also like to thank my academic advisor, Prof. Dennis Freeman for his support and suggestions over the last few years. I would also like to thank my freshman advisor, Evette Layne for she helped me out immensely during my first year. I would like to thank Anne Hunter, Vera Sayzew, Helen Schwartz, and Linda Sullivan for the support before and during this thesis. I owe my thanks also to Ron Roscoe, for allowing me to borrow equipment to use when the lab closed earlier and on weekends. I would like to thank John Sweeney, Arlin Mason and Lourenço Pires for helping me out when I was in lab. I would like to thank my family, my father Rayal, mother Yvonne, brothers Orville and Gary and my sister Vanessa for their continued support and I dedicate this thesis to them. Last but certainly not least, Franceny Bedoya. What can I say, she is my biggest supporter as she is the one that had to suffer through all the electronics and paper and books that I left around the house, the complaints by me about how the lab closed often 2 hours before its posted hours and sometimes open 2 hours after posted hours. She helped me by being there when I was frustrated about my circuit not working, and by making sure that I stayed on task.

Contents

List of Figures

List of Tables

Chapter 1

Introduction

1.1 Background and Motivation

The magnetic levitator is one of the demos used to teach linear control theory. It demonstrates how linearizing a nonlinear system along with the use of a linear controller can be used to create a stable system around an equilibrium point. The linear range for the magnetic levitator is however very small due to the method of linearization and does not allow the levitating object to move very far outside of this range. Another limiting factor is the linear range of the sensor used to determine the position of the levitating object within the magnetic field. In order to create a wide-linear range system, the system and the sensor need to be wide range.

The method of linearization most often used, is to determine the system's transfer function through a Taylor series expansion at a specific operating point and then neglect higher order terms of the state variable, along with cross products of state variable perturbations. Methods of position sensing include photo-detectors as in [7, 14], hall effect sensors as in [1, 2]. There are also variations in coil drivers as well, such as class A amplifiers in [2, 7, 14] and switching amplifiers as in [3, 9, 13].

There is an alternate method to linearize the system known as feedback linearization. The central idea of the approach is to algebraically transform the nonlinear system dynamics into a (fully or partly) linear one, so that linear control techniques can be applied. This type of linearization is achieved by exact state transformations

and feedback, rather than by linear approximations of the dynamics [11, 8]. The new transformed system is therefore operating-point invariant.

1.2 Thesis Objectives

Previous work has focused on building a levitator to illustrate the behavior of a nonlinear system around an operating point. They are not intended for moving the ball/object through space. This thesis aims to combine the methods of feedback linearization, power converter design and classical feedback design towards the implementation of a levitator/suspension system that

- is stable
- does not depend on operating point
- allows larger displacement of the object compared with a linear-approximated system
- dissipates less power in the power amplifier
- has large disturbance rejection to forces in the vertical direction

A program of analysis, circuit simulations, and experimental verification is developed to investigate the performance of the wide-linear-range magnetic levitator-and-sensor system through the use of both linear and nonlinear compensation. This work provides the analytic tools required to evaluate the usefulness of this method of linearization.

1.3 Thesis Outline

This thesis is divided into five chapters, including this introduction. The document builds up from the definition of the system to the definition of a controller to the design and implementation of the controller.

Chapter 2 reviews the modeling of the single axis magnetic levitator. It illustrates

the nonlinear behavior of the levitator, as well as its linear behavior for small motions around an operating point along with its frequency response. It also outlines experiments for parameter identification of the levitator, such as the leakage inductance, position dependent inductance, and the natural length of the electromagnet as well as the mass of the suspended object which in this case is hollow metal globe. The chapter also touches on the Taylor series expansion which defines the linear behavior from the nonlinear behavior.

Chapter 3 details the nonlinear control theory used for position control of the magnetic levitator. It introduces the concept of feedback linearization in general as well as specific to the levitator. The chapter concludes with the design of a linear compensator, specifically a lead network.

Chapter 4 details the design of useful nonlinear circuits used in this project as well as a current driver and a linear position sensor. The nonlinear circuits are based on analog multipliers.

Finally, Chapter 5 concludes the thesis with experimental results, comparisons with predicted responses as well as suggestions for future work in the subject.

Chapter 2

System Dynamics

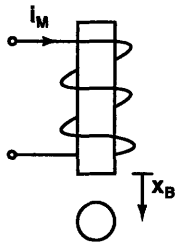

Figure 2-1: Magnetic Levitator

Before building any circuitry around the electromagnetic suspension/levitator system, the dynamics of the system have to be derived. The dynamics will dictate the gains to be used and the type of controller to be developed. The equation of motion is first derived in its nonlinear form with no approximations. The nonlinear equation is then linearized through Taylor series expansion around a nominal operating point to get the conventional linearized levitator.

2.1 Nonlinear Dynamics

The open loop dynamics of the magnetic levitator shown in Figure 2-1 is derived through co-energy techniques introduced in [15] and discussed in [6]. The important equations to take away are the inductance of the system, the magnetic energy, and

the force of the ball due to the magnetic energy.

$$L(x_B) = L_0 + \frac{L_1}{1 + \frac{x_B}{a}} \tag{2.1}$$

$$W_m = \frac{1}{2} L(x_B) i_M^2 \tag{2.2}$$

$$f_m = \frac{dW_m}{dx_B} = \frac{dL(x_B) i_M^2}{2dx_B} = -\frac{L_1 i_M^2}{2a(1 + \frac{x_B}{a})^2} \tag{2.3}$$

With the force on the ball due to the magnetic field known, the equation of motion of the ball can be defined. The only forces acting on the ball in the vertical direction are the force due to gravity downwards and the magnetic field upwards, therefore the equation of motion is:

$$f_b = Mg - f_m - f_d \tag{2.4}$$

$$M\ddot{x_B} = Mg - \frac{L_1 i_M^2}{2a(1 + \frac{x_B}{a})^2} - f_d \tag{2.5}$$

where M is the mass of the ball, g, the acceleration due to gravity and f_d is a disturbance force in the same direction as the magnetic force (gravity is a constant at one location).

The equation of motion in its full nonlinear form is therefore:

$$\dot{x_1} = x_2 \tag{2.6}$$

$$\dot{x_2} = -\frac{C}{M}\left(\frac{i_M}{x_1}\right)^2 + g - \frac{f_d}{M} \tag{2.7}$$

Here $x_1 = a + x_B$ and $C = \frac{aL_1}{2}$.

2.2 Linear Dynamics

Using the above nonlinear dynamics, the linear dynamics for small perturbations around a nominal operating are derived through Taylor series expansion. Each variable is written in terms of an operating point plus an incremental perturbation:

$x_B = X_B + x_b$ and $i_M = I_M + i_m$ and then inserted into the nonlinear equation.

$$f_M = F_M + f_m \approx f_M(I_M, X_B) + \left(\frac{df_M}{dx_B}|_{I_M,X_B}\right) x_b + \left(\frac{df_M}{di_M}|_{I_M,X_B}\right) i_m \tag{2.8}$$

$$f_M = F_M + f_m \approx -\frac{L_1 I_M^2}{2a(1+\frac{X_B}{a})^2} + \frac{L_1 I_M^2 x_b}{a^2(1+\frac{X_B}{a})^3} - \frac{L_1 I_M i_m}{a(1+\frac{X_B}{a})^2} \tag{2.9}$$

From Equation 2.7, the linearized dynamics of the ball is then

$$M\ddot{x} = Mg - \frac{L_1 I_M^2}{2a(1+\frac{X_B}{a})^2} + \frac{L_1 I_M^2 x_b}{a^2(1+\frac{X_B}{a})^3} - \frac{L_1 I_M i_m}{a(1+\frac{X_B}{a})^2} - f_d \tag{2.10}$$

If it is assumed that the operating point position X_B is realized when the force of gravity just cancels the force due to the electromagnet, i.e.

$$Mg - \frac{L_1 I_M^2}{2a(1+\frac{X_B}{a})^2} = 0 \tag{2.11}$$

then substituting this position, the linearized state equation of motion around the operating point X_B is then

$$M\ddot{x} = 2Mg\left(\frac{x_b}{a(1+\frac{X_B}{a})} - \frac{i_m}{I_M}\right) \tag{2.12}$$

And in full state space form:

$$\dot{x_1} = x_2 \tag{2.13}$$

$$\dot{x_2} = \frac{2g}{a+X_B} x_1 - \frac{2g}{I_M} i_m \tag{2.14}$$

With Equation 2.14, the linear dynamics for small perturbations around a nominal operating point is fully defined.

2.3 Levitator Parameter Identification

The parameters that are important to build the system are: the mass of the ball M, the displacement dependent inductance $L(x_B)$, and the natural length of the

electromagnet a.

The values for the mass of the metal globe M, coil resistance R, and L are easily determined. The globe was measured, not by the author but by providers of the globe from LNS Technologies, which sells a levitator kit. The value of R is measured using a multimeter and the value of L, specifically $L(x_B)$ is determined by measuring the time constant of the coil current response to a voltage step outlined in the following experiments.

2.3.1 Experiments

L_0 Drive the inductor with a square wave of voltage that is slow enough for the inductor current to settle. The inductor current should look like the Figure 2-2.

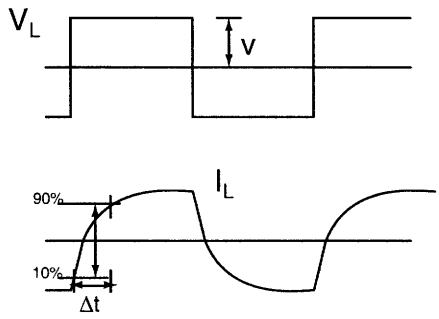

Figure 2-2: Illustration of rise time measurements

Measure and record the $10\% - 90\%$ rise time for the case when the ball is absent from the magnetic field, i.e. $x_B = \infty$.

L_1 Repeat the above experiment for the case when the ball is touching the face of the electromagnet, i.e. $x_B = 0$.

a Repeat the experiment a third time with the ball an arbitrary distance $x_B = x_a$ from the face of the electromagnet such that the inductance is in between L_0 and L_1. Using the values for L_0 and L_1 found above, solve for a and record.

2.3.2 Measurements

The measurements for the system studied in this document are tabulated below in Table 2.1.

Parameter	Units	Value
mass of metal ball	M [kg]	3.15×10^{-3}
coil resistance	$R[\Omega]$	13.7
coil inductance	$L_0[mH]$	213
coil inductance	$L_1[mH]$	19.2
constant	$a[m]$	4×10^{-3}
maximum coil applied voltage	$v_{MAX}[V]$	15

Table 2.1: Electromagnet System Parameters

Chapter 3

Nonlinear Control Theory

3.1 Overview

This chapter introduces the theory used to construct the position controller for the magnetic levitator. In Chapter 2 it is realized that the levitator system is nonlinear. Therefore, in order to operate over a wide range of inputs, the system needs to be transformed into a linear system. This is done through feedback linearization.

3.2 Feedback Linearization

The central idea of the approach is to algebraically transform the nonlinear system dynamics into a (fully or partly) linear one, so that linear control techniques can be applied. The resulting system is an equivalent model, just in simpler form. The new transformed system is however operating-point invariant. The concept is illustrated in Figure 3-1 below.

The system is constructed in two loops, the linearization loop and the pole-placement loop. The purpose of the linearization loop is to transform the nonlinear system dynamics represented by

$$\dot{x} = f(x, u) \tag{3.1}$$

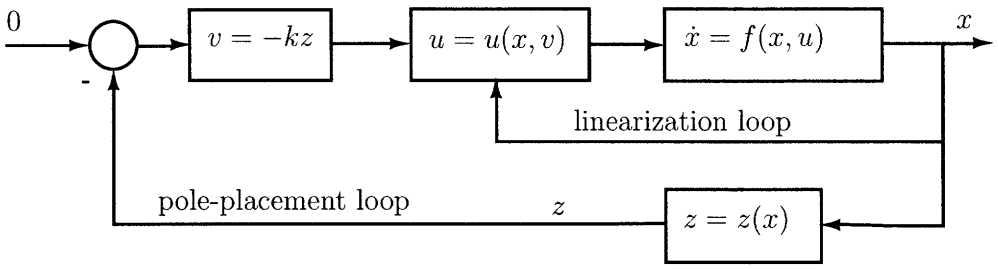

Figure 3-1: Input-state linearization

into a linear system with the help of a nonlinear compensator represented by $u = u(x, v)$. The purpose of the pole-placement loop is to compensate the resulting linear system for a desired frequency response with the help of the linear compensator represented by $v = -kz$. The term z is a measure of the output variable as with a sensor. Specifically in this project the drive u is the electromagnet current represented by i_M, and the output variable is the position of the ball represented by x_1.

3.2.1 Nonlinear Compensator

The nonlinear compensator creates an operating point independent system by compressing the input drive by the inverse of the system's nonlinearity. What this means is that the electromagnet is driven with the "correct" current for a given displacement/position of the ball. The "correct" current generates an electromagnetic force that balances the force due to gravity at a given position. The design of this current is based on the nonlinear dynamics introduced in Chapter 2, repeated below neglecting the disturbance force.

$$\dot{x_1} = x_2 \tag{3.2}$$

$$\dot{x_2} = -\frac{C}{M}\left(\frac{i_M}{x_1}\right)^2 + g \tag{3.3}$$

If the nonlinear term $\frac{C}{M}\left(\frac{i_M}{x_1}\right)^2$ is set to some new control v, it is then apparent that if the coil current is made to vary as

$$i_M = x_1\sqrt{\frac{M}{C}v} \tag{3.4}$$

for the new control v, then the levitator is globally linearized and operating point invariant. Equation 3.4 represents the full nonlinear compensator. This compensator is implemented here in analog hardware where signals will be represented by voltages and currents. If the compensator is represented in the form:

$$V_M = \frac{V_x\sqrt{k_n v}}{k_m} \tag{3.5}$$

$$i_M = \frac{V_M}{R_M} \tag{3.6}$$

it can then be constructed with analog multipliers such as Analog Devices AD633. In this case the system's block diagram is represented in Figure 3-2, where V_x is the position of the ball in units of volts $[V]$, R_M is a resistance in units of ohms $[\Omega]$, k_n and k_m are constants, intrinsic to the multiplier, in units of volts $[V]$, and k_x is the sensor gain in units of volts per meter $[\frac{V}{m}]$.

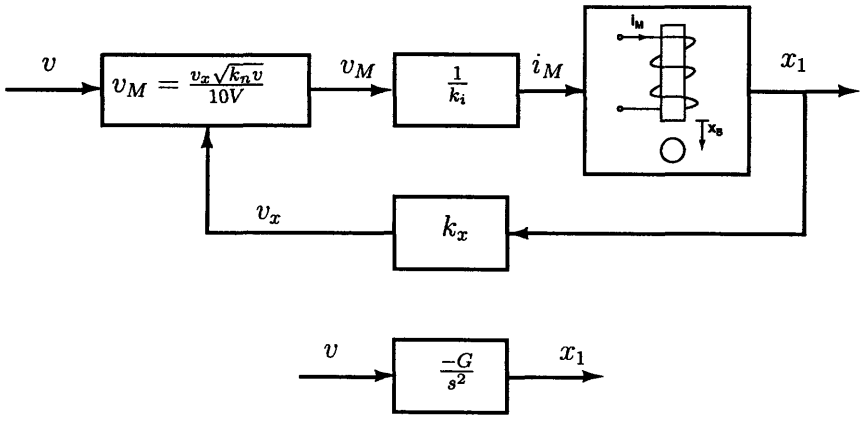

Figure 3-2: Nonlinear magnetic suspension system

The system is now linearized and represented by the state equations

$$\dot{x_1} = x_2 \tag{3.7}$$

$$\dot{x_2} = -\left(\frac{Ck_x^2k_n}{Mk_m^2R_M^2}\right)v + g \tag{3.8}$$

and transfer function:

$$\frac{X_1(s)}{V(s)} = \left(\frac{Ck_x^2k_n}{Mk_m^2R_M^2}\right)\frac{1}{s^2} \tag{3.9}$$

free from any operating point constraints. The new plant from v to x_1 is represented by a double integrator with a gain $G = \frac{Ck_x^2k_n}{Mk_m^2R_M^2}$. The system parameters are listed in Table 3.1. Assuming that the transformation is correct and the new system is fully represented by Equation 3.9, a linear compensator must now be designed to make the system unconditionally stable. The linear compensator is represented by $G_c(s)$ in Figure 4-2. The usual linear control techniques can then be employed to create a stable robust system that is trackable.

Parameter	Units	Value
current driver trans-resistance	$R_M[\Omega]$	4
magnetic force constant	$C[\frac{Nm^2}{A^2}]$	3.84×10^{-5}
sensor gain	$k_x[\frac{V}{m}]$	235
square-root gain	$k_n[V]$	10
multiplier gain	$k_m[V]$	10

Table 3.1: System Parameters

To implement the nonlinear compensator represented by Equation 3.4 in circuit form, both a multiplier and a square-root circuit are required. The circuit implementation of these circuits are discussed in the next chapter.

3.2.2 Linear Compensator: Lead Compensation

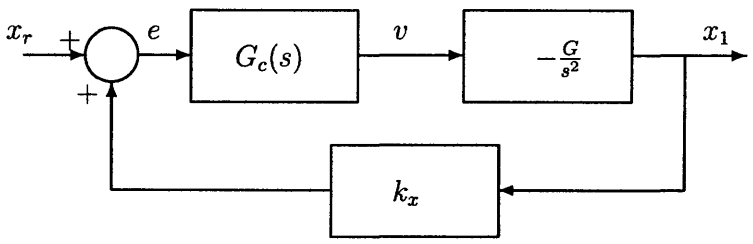

Figure 3-3: Feedback linearized block diagram

The design of the linear compensator is based on the linearized system represented by the transfer function in Equation 3.9 whose frequency response is shown in Figure 3-4. The uncompensated system has zero phase margin for the phase is -180^o at all frequencies. In order for the system to be unconditionally stable, it requires a positive phase margin and a large gain margin.

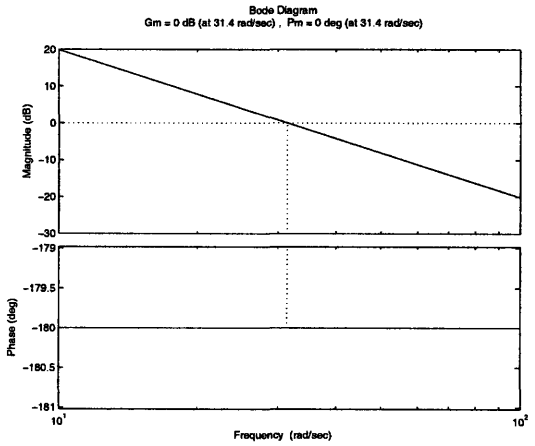

Figure 3-4: Bode Plot of Open Loop Uncompensated System

This can be accomplished with the lead compensator. Lead compensation provides maximum phase margin at the geometric mean of the compensator. The lead compensator has the form:

$$G_c(s) = K_L\left(\frac{\alpha\tau_L s + 1}{\tau_L s + 1}\right) \tag{3.10}$$

The compensator is comprised of a single pole and a single zero which is located at a frequency below the pole. The system can be compensated without changing the low-frequency behavior with maximum phase margin by placing the compensated crossover frequency at the geometric mean of the lead-compensator [6]. Typically $\alpha = 10$ is chosen as a trade-off between maximum phase bump and high frequency noise rejection. The maximum phase bump is given by:

$$\phi_B = \arcsin\left(\frac{\alpha - 1}{\alpha + 1}\right) \tag{3.11}$$

with a phase bump of $\phi_B = 55^o$ for $\alpha = 10$. Along with $\alpha = 10$, the other design criteria for the system are 55^o of phase margin and a crossover frequency less than 10Hz. The loop transmission for the compensated system shown in Figure 3-3 is:

$$L(s) = K_L\left(\frac{10\tau_L s + 1}{\tau_L s + 1}\right)\frac{998}{s^2} \tag{3.12}$$

If K_L is chosen to be 1, then the crossover frequency without the compensator is:

$$\omega_u = 31.6 \text{ rps} = 5\text{Hz} \tag{3.13}$$

In order to satisfy the requirements above, the lead-zero is placed a factor of $\sqrt[4]{\alpha}$ below the former crossover ω_u. Therefore,

$$\frac{1}{10\tau_L} = \frac{\omega_u}{\sqrt[4]{\alpha}} \tag{3.14}$$

and

$$\tau_L = \frac{\sqrt[4]{\alpha}}{10\omega_u} = 5.6 \text{ ms} \tag{3.15}$$

The full compensator is therefore represented by

$$G_c(s) = \left(\frac{0.056s + 1}{0.0056s + 1}\right) \tag{3.16}$$

with $K_L = 1$ abstracted into the uncompensated loop gain. The fully compensated

system's loop gain is therefore

$$L(s) = \frac{998}{s^2}\left(\frac{0.056s+1}{0.0056s+1}\right) \tag{3.17}$$

and the frequency response and step response are presented in Figures 3-5 and 3-6 respectively.

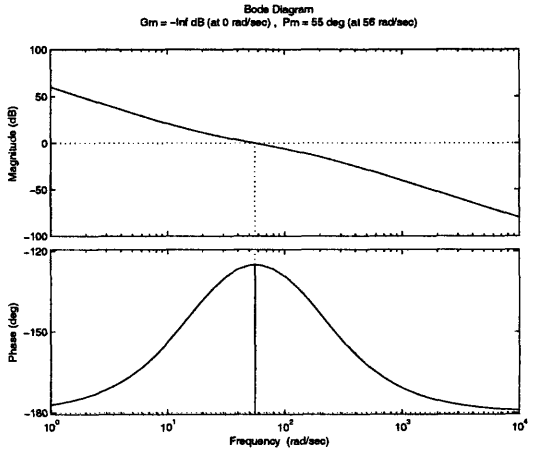

Figure 3-5: Bode plot of lead-compensated system

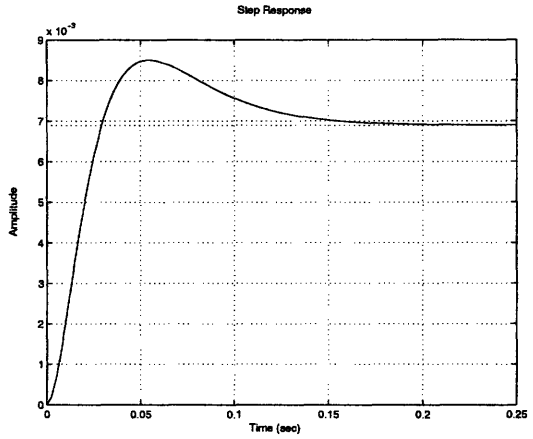

Figure 3-6: Step response of lead-compensated system

The compensated system has a new crossover frequency of 56 rps = 8.9 Hz with a phase margin ϕ_M of 55°. This translates into a step response with a 20% peak overshoot. A step input of 2.35 V commands a displacement of $x_1 = 1$ cm.

The circuit implementation of a lead compensator can be constructed as shown in Figure 3-7. The transfer function from V_{in} to V_{out} is:

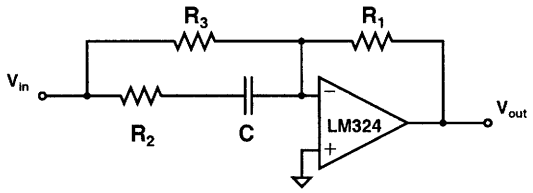

Figure 3-7: Implementation of a Lead Compensator

$$\frac{V_{out}}{V_{in}} = -\left(\frac{R_1}{R_3}\right)\frac{(R_2+R_3)Cs+1}{R_2Cs+1} \tag{3.18}$$

To design the lead compensator, the value of the capacitor is chosen to be $C = 1\mu F$. Since $\tau = R_2C = 5.6$ms, the value of R_2 is therefore:

$$R_2 = \frac{\tau}{C} = 5.6\ k\Omega \tag{3.19}$$

and a value of $\alpha = 10$ determines R_3 to be:

$$R_3 = 9 \cdot R_2 = 50.4\ k\Omega \tag{3.20}$$

while a gain of 1 determines the value of R_1 to be:

$$R_1 = R_3 = 50.4\ k\Omega \tag{3.21}$$

For all resistors, the nearest 5% values are used, which are: $R_2 = 5.6\ k\Omega$, $R_3 = R_1 = 51\ k\Omega$.

Chapter 4

Hardware Implementation

4.1 Overview

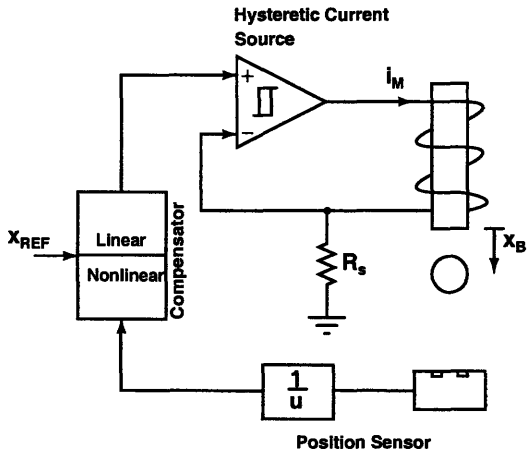

Figure 4-1: Levitator control system

This chapter details the design of a position controller based on the nonlinear dynamics developed Chapter 2 and nonlinear controller defined in Chapter 3. The basic topology is shown in Figure 4-1. The controller is comprised of a linear position sensor, a hysteretic current source, a nonlinear compensator and finally a linear compensator.

The position sensor uses a OPB732 reflective switch at its core. It contains a

photodiode, used to generate an infrared light source and a phototransistor, used to detect the light, in one package. The metal ball is suspended above the sensor which produces a current that nonlinearly depends upon the position of the ball. The current is driven into a resistor to get a voltage dependent on position and then linearized with a divider. This resulting voltage is used by nonlinear compensator to linearize the force to drive relationship and by the linear compensator to drive the current source.

A block diagram of the topology is shown in Figure 4-2

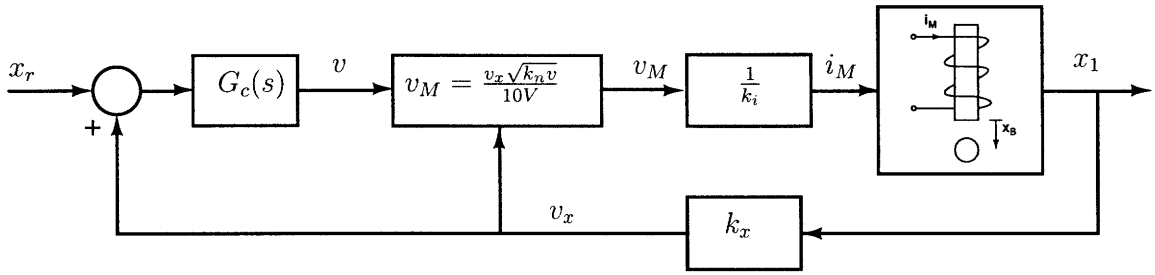

Figure 4-2: Nonlinear compensation of magnetic suspension system

where $G_c(s)$ represents the linear compensator, $v_M = \frac{v_x\sqrt{k_n v}}{10V}$ $[V]$ represents the nonlinear compensator, k_n $[V]$ is a constant, k_i $[\Omega]$ represents the current source, and k_x $[\frac{V}{m}]$ represents the position sensor. The symbols in brackets represent the units of each constant, i.e., the units of k_x is volts per meter. The exact values of each symbol is presented in the subsequent sections.

4.2 Multipliers, Dividers and Square-Rooters

The following nonlinear circuits are useful in compensating nonlinearities. These circuits are based on analog multipliers, specifically Analog Devices's AD633 and AD532 multipliers. Both multipliers have the same transfer function, namely

$$V_{out} = \frac{(\mathrm{X_1} - \mathrm{X_2})(\mathrm{Y_1} - \mathrm{Y_2})}{10V} \tag{4.1}$$

with the only difference is that the AD532 has an internal operational amplifier shown below in Figure 4-3.

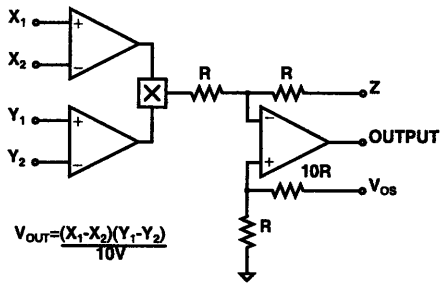

Figure 4-3: Analog Devices AD532

Division is frequently accomplished by applying feedback around an analog multiplier. Since the AD532 multiplier comes with an internal op amp it is immediately ready for such an implementation.

In order to implement a divider, the output of the amplifier is connected to one of the multiplier inputs as shown in Figure 4-4.

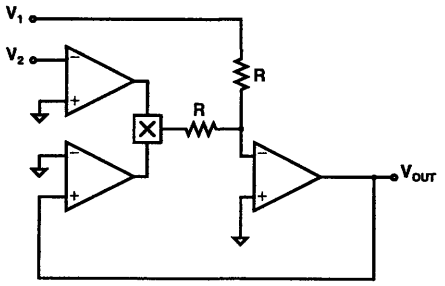

Figure 4-4: Divider implemented with the AD532

The large gain of the op amp and negative feedback forces the terminals of the op amp to be equal. Therefore:

$$\frac{-V_{OUT}V_2}{10V \cdot R} + \frac{V_1}{R} = 0 \tag{4.2}$$

and therefore

$$V_{OUT} = \frac{10V \cdot V_1}{V_2} \tag{4.3}$$

The square-rooting function can be implemented in a similar way. To implement, the output of the op amp is shorted to both inputs of the multiplier as shown in Figure 4-5.

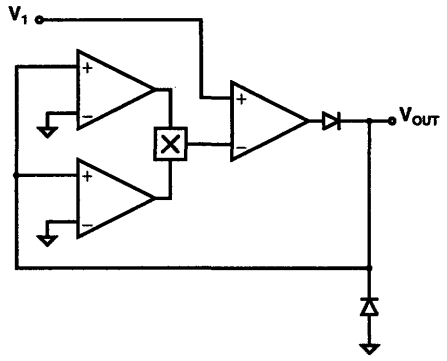

Figure 4-5: Square-rooter implemented with the AD633

As before, the large gain of the op amp and negative feedback forces the terminals of the op amp to be equal. Therefore:

$$V_{OUT} = a(s)(V_1 - \frac{V_{OUT}V_{OUT}}{10V}) \tag{4.4}$$

and therefore

$$V_{OUT} = \sqrt{10V \cdot V_1} \quad V_1 > 0 \tag{4.5}$$

4.3 Position Sensor

4.3.1 Overview

OPTEK Technology's long distance reflective switch (OPB732) was the choice of position sensor for the levitator. The OPB732 uses an infrared light-emitting-diode (LED) and phototransistor in a reflective switch configuration. While an object is in the reflective path of the sensor, light from the LED will be reflected back to the housing irradiating the surface (base) of the phototransistor. When infrared light strikes the phototransistor, the transistor becomes forward biased, [10] just as a reg-

ular bipolar junction transistor, with the infrared light operating as the base current. The OPB732 offers both the emitter and detector in one package allowing easy integration.

4.3.2 Design

Since the reflective switch emits infrared light to determine determine the presence of an object, it would appear that the sensor is susceptible to the same problems as previous photo-detector circuits, that being the presence of infrared radiation in ambient light mainly from the 60 Hz in the surrounding lights. The opaque housing of the sensor however reduces this interference. A quick look at the spectral density or FFT of the returning signal however shows that the 60 Hz frequency and its harmonics are absent from the signal. This means that no additional filtering is required.

The sensor does however have a nonlinear distance to current relationship. This nonlinear relationship is quantified using the circuit in Figure 4-6.

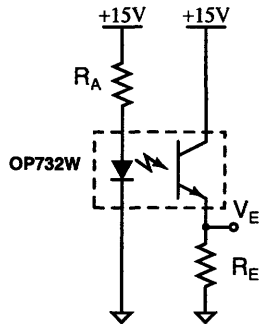

Figure 4-6: Circuit used to measure current to distance relationship of the OP732W reflective switch

The typical forward drop of the diode is 1.8 [V] and has an absolute maximum peak forward current of 1 [A] and a maximum DC forward current of 50 [mA]. A forward current of 30 [mA] was chosen for this project. The resistor R_A sets the current in the diode. The value of the resistor is therefore:

$$R_A = \frac{15\text{V} - 1.8\text{V}}{30\text{mA}} = 440\ \Omega \tag{4.6}$$

The nearest 5% resistor used in this implementation is $R_A = 430$ [Ω]. The phototransistor has a maximum collector DC current of 50 [mA] and has a collector-emitter saturation voltage of 0.4 [V]. The collector current chosen was also close to 30 [mA]. The value of resistor is therefore:

$$R_E = \frac{15\text{V} - 0.4\text{V}}{30\text{mA}} = 487\ \Omega \tag{4.7}$$

The actual resistor used in this implementation is $R_E = 510$ [Ω]. With this implementation, the voltage representation of position is measured at the emitter of the phototransistor. The result of the experiment is displayed below in Figure 4-7

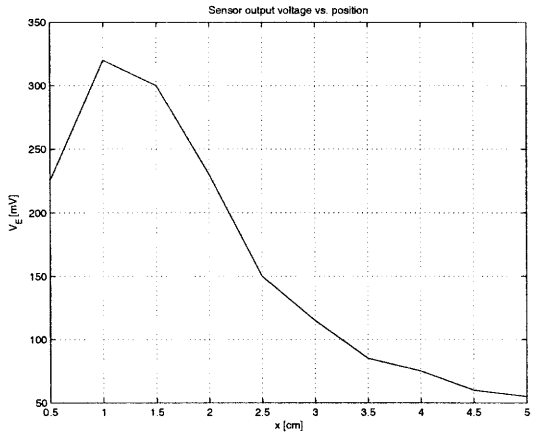

Figure 4-7: Position sensor output voltage vs. position

This nonlinearity needs to be corrected to allow a wide linear range sensor. It is apparent that the nature of the nonlinearity is hyperbolic with respect to the distance of the detected object from the sensor. The output voltage V_E at the emitter of the phototransistor can be represented in the form:

$$V_E(x_B) = \frac{k}{x_B - x_0} \tag{4.8}$$

where k is a gain of 1.63×10^{-3} [Vm], x_B is the distance of the ball from the sensor, and x_0 of 1.5 [cm] is an offset which is due to the fact that if the object is too close, there is zero reflection/detection.

The sensor data fitted with Equation 4.8 for $x_B \geq 1.5$ [cm] is shown in Figure 4-8 below. The only error with the fit is at low ball position, i.e. when the ball is closer than 2 [cm] to the sensor.

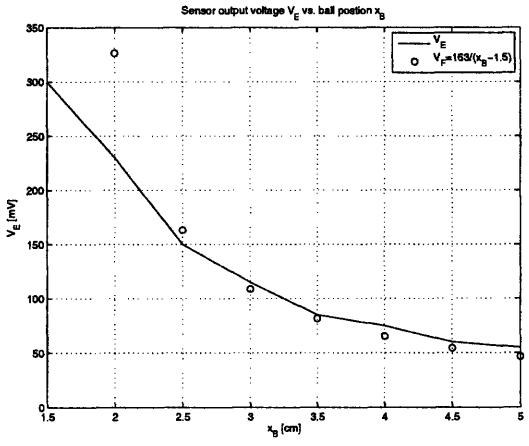

Figure 4-8: Position sensor output voltage vs. position fitted with Equation 4.8

In order to get a linear response from the sensor, the inverse of the sensor output needs to computed. This can be most easily achieved through the use of an analog divider. Using the divider of Equation 4.3 with V_1 set to a constant voltage and V_2 equal to V_E, the new theoretical sensor output voltage is therefore:

$$V_s(x_B) = \frac{10 \cdot V_1[V]^2}{V_E(x_B)} = \frac{10V \cdot V_1}{k}(x_B - x_0) \tag{4.9}$$

which is linear in x_B. The theoretical linearized sensor characteristic is shown below in Figure 4-9. If the constant voltage is set to $V_1 = 1.4$ and the previous sensor voltage is multiplied by a gain of thirty then the linearized sensor follows the equation below, where V_{sen} is in volts [V], x_B is in centimeters [cm] and gain is $k_x = 2.35$ $[\frac{\mathrm{V}}{\mathrm{cm}}]$.

$$V_{sen} = 2.35x_B - k \tag{4.10}$$

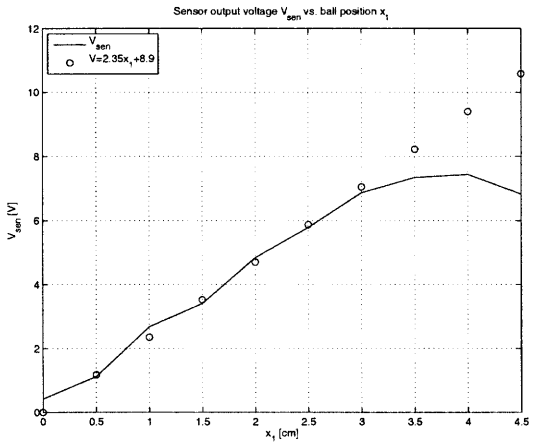

Figure 4-9: Linearized position sensor output voltage vs. position

4.3.3 Experimental Implementation

The circuit implementation of the linearized sensor is shown in Figure 4-10. The circuit consists of the OPB732 reflective switch, an AD620 instrumentation amplifier configured for a gain of thirty, the AD532 configured as a divider and another instrumentation to provide a voltage offset, since the result of the divider are negative voltages. The result is a sensor output voltage which increases as the ball moves away from the electromagnet pole (increasing x_1). There is a 5-cm gap between the electromagnet and the sensor and the ball has a diameter of 2.54-cm, therefore the ball should have a theoretical maximum displacement of 1-cm before moving out of the linear range of the sensor as shown in Figure 4-9

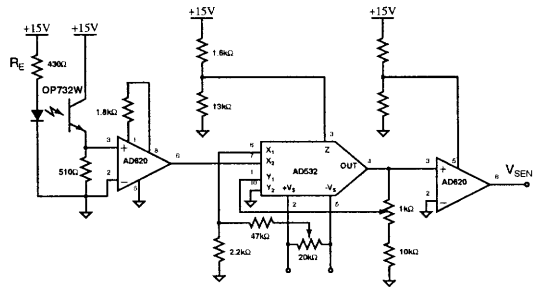

Figure 4-10: Circuit implementation of position sensor

4.4 Current Driver

4.4.1 Overview

The design of the current driver of Figure 4-2 is discussed in detail in this section. The driver is implemented as a hysteresis controlled DC-to-DC switching power converter, specifically a buck converter [4]. The motivation for the use of a switching amplifier is efficiency and the presence of an inductive filter provided by the inductance and resistance of the electromagnet. The use of a buck converter is preferred because the inductor or electromagnet current is linearly proportional to the input voltage, derived in the next section.

A switching power converter has a theoretical efficiency of 100% because it is made up of ideal lossless elements such as capacitors, inductors and switches. Although in the real world such a high efficiency is not possible due to finite switching times of the switches which will be discussed later, and that of equivalent series resistances (ESR) of capacitors and inductors, switching amplifiers are much more efficient than linear ones. More efficiency means less power is dissipated as heat in the devices and more power is transferred to the load, which in this case is the electromagnet.

4.4.2 Buck Converter

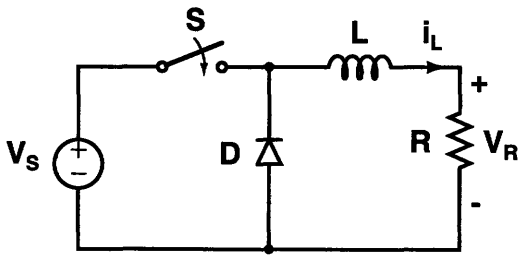

Figure 4-11: Basic Buck Converter

The steady state operation of the buck converter is determined through periodic steady state analysis. In periodic steady state, the system returns to the same point at the end of every switching cycle [4]. Over one cycle, the switch is on for a time DT

and off for a time $(1-D)T$, where D is the duty ratio which is the ratio of the time that the switch is on, to the period T, which is the one over the switching frequency. Specifically, under periodic steady state conditions, the average voltage across the inductor L in Figure 4-11 is zero.

$$\langle V_L \rangle = \int_0^T V_L dt = 0 \tag{4.11}$$

$$V_L = \begin{cases} V_s - i_L R & \text{if } 0 < t \leq DT \\ -i_L R & \text{if } DT < t \leq T \end{cases} \tag{4.12}$$

$$\langle V_L \rangle = \int_0^{DT} (V_s - i_L R) dt - \int_{DT}^T i_L R = 0 \tag{4.13}$$

$$\langle V_L \rangle = (V_s - i_L R)DT - i_L R(1-D)T = 0 \Rightarrow \tag{4.14}$$

$$i_L = \frac{D}{R} V_s \tag{4.15}$$

It is clear from Equation 4.15 that the current through the electromagnet can be controlled by varying the duty ratio D, assuming V_s and R are constants.

4.4.3 Hysteretic Control

The method of control chosen for the buck converter/current driver is that of hysteretic control mainly to satisfy the requirement that the current driver be much faster than the overall open loop system. In hysteresis control, switching boundaries are defined in terms of a single state variable, or the system output, i.e. inductor current. Two boundaries with a small separation control the switch S turn-on and turn-off action [5]. The concept is illustrated in Figure 4-12 below.

During the time DT or t_1, when the switch is on, the inductor current increases with a time constant $\tau = \frac{L}{R}$. Conversely, during the time $(1-D)T$ or t_2, when the switch is off, the inductor current decreases with the same time constant. It is clear then that the switching frequency, defined as $f_{sw} = \frac{1}{T}$ and the duty ratio defined as $D = \frac{t_1}{T}$ are defined by the time constant τ and the hysteresis band $V_h = V_B - V_A$.

A detailed analysis of the switching frequency and duty ratio dependence is derived and summarized below.

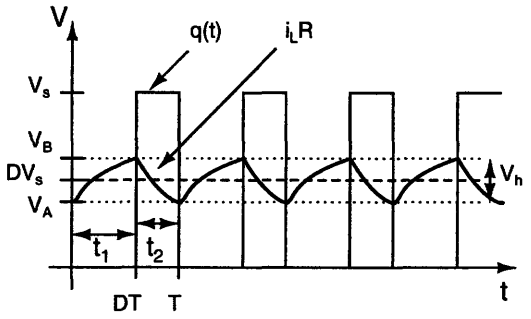

Figure 4-12: Transient response of hysteresis controlled buck

During time t_1, the switch is on and the diode is off, and therefore the inductor current i_L, the voltage across the resistor V_R and t_1 are:

$$i_L = \frac{V_s}{R}(1 - e^{-\frac{t}{\tau}}) \tag{4.16}$$

$$V_R = V_s(1 - e^{-\frac{t}{\tau}}) \tag{4.17}$$

$$t_1 = -\tau \ln\left(\frac{V_B - V_s}{V_A - V_s}\right) = \tau \ln\left(\frac{V_s - V_A}{V_s - V_B}\right) \tag{4.18}$$

While during time t_2, the switch is off and the diode is on and the current in the inductor i_L, the voltage across the resistor V_R and t_2 are:

$$i_L = \frac{V_B}{R} e^{-\frac{t}{\tau}} \tag{4.19}$$

$$V_R = V_B e^{-\frac{t}{\tau}} \tag{4.20}$$

$$t_2 = -\tau \ln\left(\frac{V_A}{V_B}\right) = \tau \ln\left(\frac{V_B}{V_A}\right) \tag{4.21}$$

The switching frequency is:

$$f_{sw} = \frac{1}{t_1 + t_2} \tag{4.22}$$

4.4.4 Experimental Implementation

The actual implementation of the hysteresis-controlled-buck-converter-based current source is shown in Figure 4-13. The circuit consists of the basic buck converter topology, an op amp used as a comparator with hysteresis for the switching and an op amp gain stage.

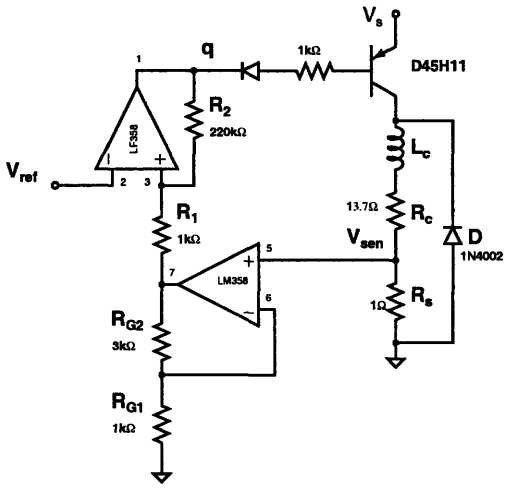

Figure 4-13: Hysteresis controlled buck converter

The analysis of the circuit is straight forward and for the most part was completed in the last section. The average inductor current is found as before as:

$$\langle V_L \rangle = (V_s - i_L(R_c + R_s))DT - i_L(R_c + R_s)(1 - D)T = 0 \tag{4.23}$$

while feedback forces pins 2 and 3 to be equal

$$V_{ref} \simeq 4V_{sen} \tag{4.24}$$

which results in an inductor current as

$$i_L = \frac{DV_s}{4R_s} = \frac{V_{ref}}{4} \tag{4.25}$$

The only item remaining is to quantify the values V_A and V_B from this topology.

The comparator output q switches to the positive supply when the positive terminal $V+$ is greater than the negative terminal $V-$ and conversely to the negative supply when the opposite is true. The voltage at the positive and negative terminals are:

$$V+ = \left(\frac{R_{G1}+R_{G2}}{R_{G1}}\right)\left(\frac{R_2}{R_1+R_2}\right)\left(\frac{R_s}{R_s+R_c}\right)V_R + \frac{R_1}{R_1+R_2}q \tag{4.26}$$

$$V- = V_{ref} \tag{4.27}$$

$$V_R = i_L(R_c+R_s) \tag{4.28}$$

To get the quantity V_A, assume that the output of the comparator q was previously high, in this case zero ($q = V_s$). The threshold that the sense voltage $V_{sen} = i_L R_s$ must exceed to turn off the switch on is:

$$V_A = \left(\frac{R_{G1}}{R_{G1}+R_{G2}}\right)\left[\left(\frac{R_2+R_1}{R_2}\right)V_{ref} - \left(\frac{R_1}{R_2}\right)V_s\right] \tag{4.29}$$

while if the output of the comparator q was previously low ($q = 0$), the threshold that the sense voltage $V_{sen} = i_L R_s$ must then fall below to turn the switch on is:

$$V_B = \left(\frac{R_{G1}}{R_{G1}+R_{G2}}\right)\left(\frac{R_2+R_1}{R_2}\right)V_{ref} \tag{4.30}$$

Combining Equations 4.22, 4.29 and 4.30, the switching frequency for this topology is:

$$f_{sw} = \frac{1}{\tau \ln\left(\frac{\frac{V_s}{k_1 k_2 V_{ref} - k_3 V_s} - 1}{\frac{V_s}{k_1 k_2 V_{ref}} - 1}\right)} \tag{4.31}$$

The most important item to take away from this analysis is that the switching frequency with respect to V_{ref} is much higher than the crossover frequency of the magnetic levitator system. This is illustrated below in Figure 4-14.

The switching frequency of the current source has a parabolic response to control voltage with the maximum switching frequency at 50 % duty ratio or $V_{ref} = 30$ or $i_L = \frac{V_{ref}}{4\Omega} = 7.5$ A. The current source will not run at such high currents as the 3-g ball only theoretical requires $i_L = 680$ mA at $x_1 = 2.4$cm. Therefore the current

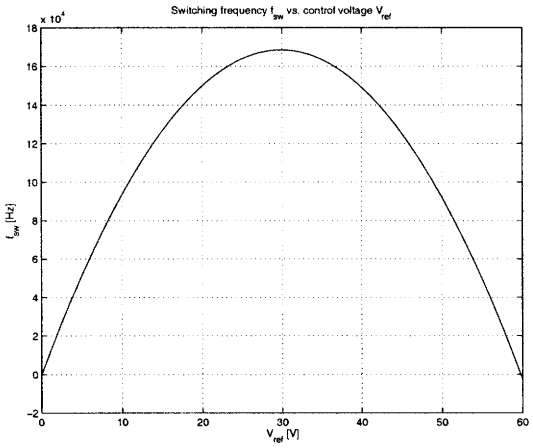

Figure 4-14: Buck switching frequency versus V_{ref}

source will always run below maximum frequency but at a higher frequency than the crossover frequency of the levitator.

Chapter 5

Results and Conclusions

This chapter presents the results of the experiments performed on the single degree of freedom magnetic levitator described in this thesis. In Section 5.1 the experimental step responses are presented and compared with responses predicted in simulation and possible sources of discrepancies are discussed. In Section 5.2 conclusions are drawn from the data presented, the thesis is summarized and suggestions for future work is discussed.

5.1 Step Responses of Levitator

This section presents and analyzes experimental step responses performed on the complete magnetic levitator. The sensor output is measured for step sizes of 100, 200, 300, 400, and 500 [mV] across two operating points and presented below in the following figures.

The results suggest that the nonlinear compensator works well at an operating point of $V_{dc} = -3$V since a linear increase in input voltage produces a linear increase in output position. There was a problem however as an operating point of $V_{dc} = -4$V exhibited very different step responses. The loop gain obviously changed for the effect of the pole-zero doublet is more apparent at $V_{dc} = -4$V.

The culprit was discovered to be the biasing of the position sensor, specifically in the instrumentation amplifier. The reason why the position sensor is bias dependent is because the V_{ref} pin is biased with a high impedance voltage source implemented as a 500kΩ potentiometer. The internal schematic of the AD620, taken from the Analog Devices data-sheet is shown below in Figure 5-16.

The V_{ref} pin is connected through a 10kΩ resistor to the output amplifier. The voltage at the positive terminal for $V_{ref} = 8.9$V is then:

$$V_+ = \frac{10k\Omega}{140k\Omega}V(x_1) + \frac{10k\Omega}{140k\Omega}V_{ref} \tag{5.1}$$

and therefore the output voltage V_{sen} is then:

$$V_{sen} = \frac{20k\Omega}{140k\Omega}V(x_1) + \frac{20k\Omega}{140k\Omega}V_{ref} \tag{5.2}$$

It is clear then that if the position dependent voltage $V(x_1)$ ranges from 0 to 8 V within the operating range of the sensor, the output voltage V_{sen} varies by position and therefore the gain of the sensor varies by position.

There are two ways to combat this problem: (1) bypass the V_{ref} pin with a large capacitor or (2) put a buffer in between the potentiometer and V_{ref}, shown in Figure 5-17 below.

The problem was discovered close to the conclusion of the thesis and therefore there was no time to correct, but if the position sensor's gain is constant through its operating range, the levitator would operate well over this region.

5.2 Conclusions and Suggestions for Future Work

The data presented in this thesis demonstrates the effectiveness of of a nonlinear compensator to linearize a nonlinear system as the step responses are essentially operating point independent within the full range of the levitator. Feedback linearization, along with a linear compensator and a linear sensor, is therefore a viable method of nonlinear control when operating over a wide range is desired.

5.2.1 Thesis Summary

The principal effort of this thesis is the design and evaluation of nonlinear analog compensators and system limitations due to sensor characteristics. A nonlinear compensator is designed which allows the magnetic system to be operating point invariant. A reflective switch positioned under the ball is used as the position sensor. The effectiveness of feedback linearization is demonstrated as the linear range of the system is increased within a small range where the position sensor's gain is not changing.

5.2.2 Suggestions for Future Work

The one difference discovered in literature was with the modeling of the inductance of the levitator using coenergy techniques. In [7, 9, 11, 15], and in this thesis, the inductance is modeled as having a hyperbolic characteristic, while [3] models it as a decaying exponential. While an exponential has a the same decaying characteristic, an inverse exponential nonlinear compensator can be investigated for future discussions on this topic.

Putting the lead compensator in the feedback loop as opposed to the forward loop is another area to explore. The system will have the same loop gain but will exhibit no overshoot.

Since the sensor was a large part of the thesis, the exploration of more efficient sensor designs should be explored. The range garnered by the linearization of the position sensor presented in this thesis was not large. The goal for future work is

to have a sensor that has a linear region larger than the maximum output current of current source. The limitations in that scenario would be the maximum current output.

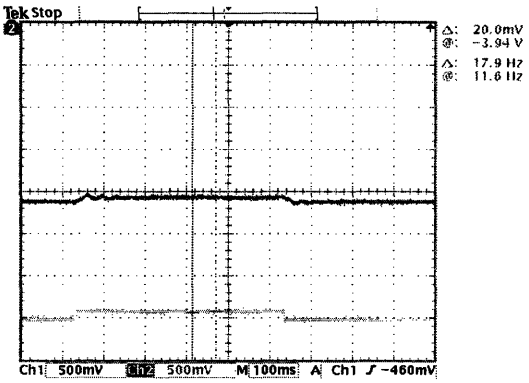

Figure 5-1: $V_{dc} = -4$V, with a square wave input of 100mVpp

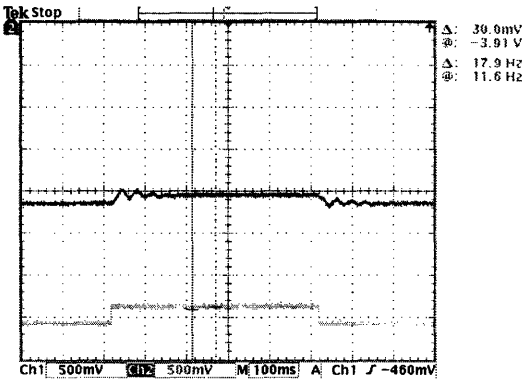

Figure 5-2: $V_{dc} = -4$V, with a square wave input of 200mVpp

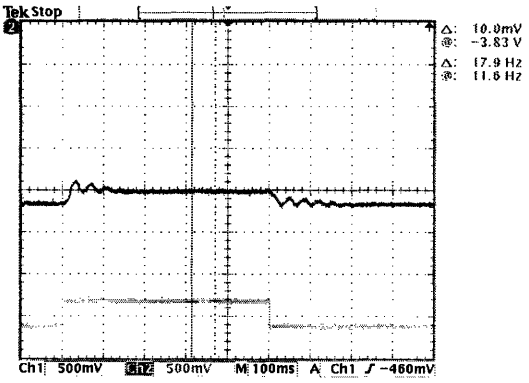

Figure 5-3: $V_{dc} = -4$V, with a square wave input of 300mVpp

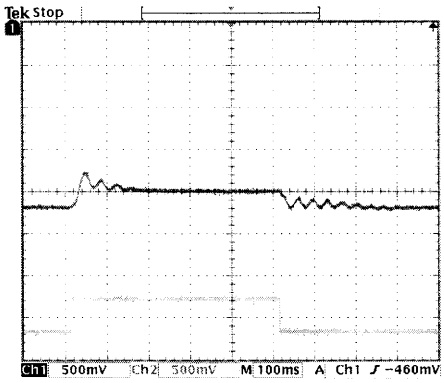

Figure 5-4: $V_{dc} = -4$V, with a square wave input of 400mVpp

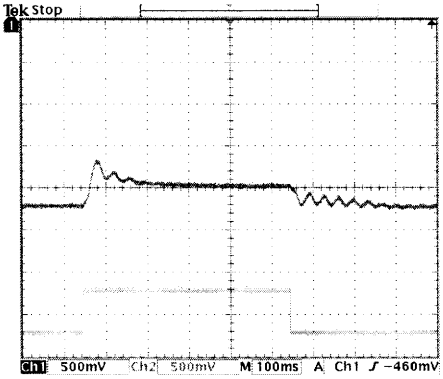

Figure 5-5: $V_{dc} = -4$V, with a square wave input of 500mVpp

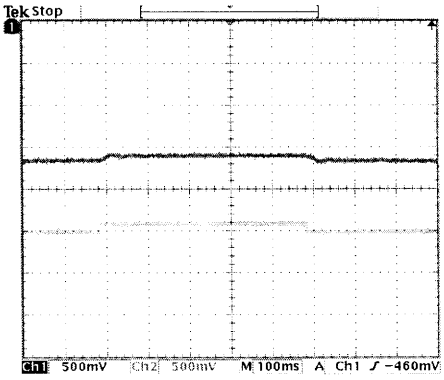

Figure 5-6: $V_{dc} = -3$V, with a square wave input of 100mVpp

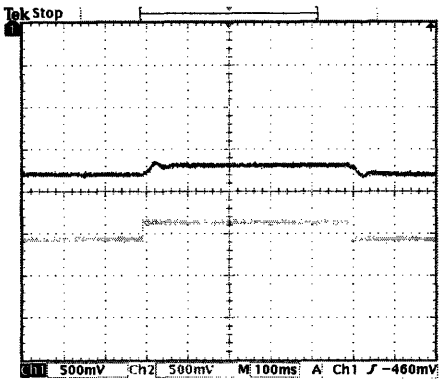

Figure 5-7: $V_{dc} = -3$V, with a square wave input of 200mVpp

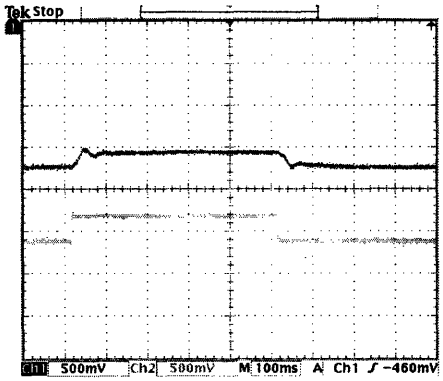

Figure 5-8: $V_{dc} = -3$V, with a square wave input of 300mVpp

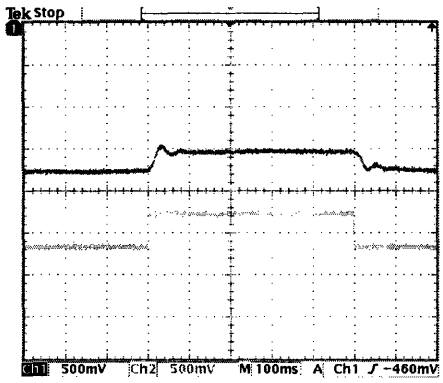

Figure 5-9: $V_{dc} = -3$V, with a square wave input of 400mVpp

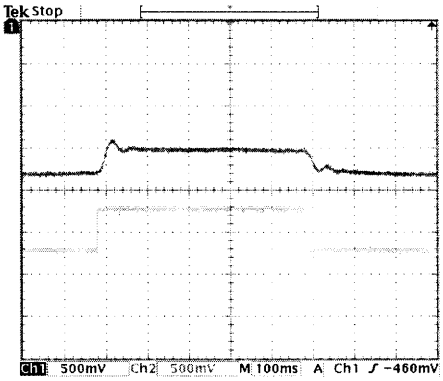

Figure 5-10: $V_{dc} = -3$V, with a square wave input of 500mVpp

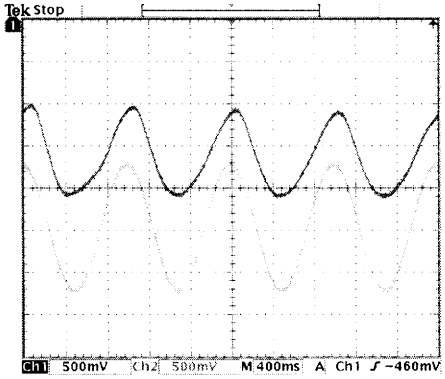

Figure 5-11: $V_{dc} = -3$V, with a sine wave input of 1.5Vpp

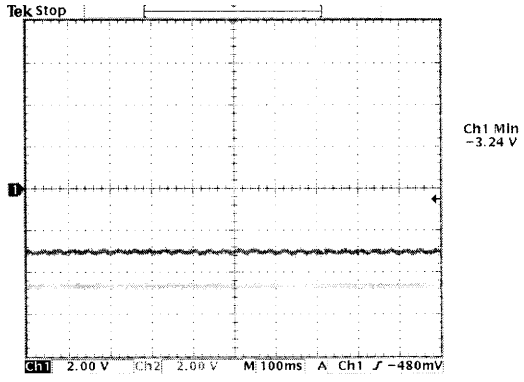

Figure 5-12: Minimum input voltage for the levitator

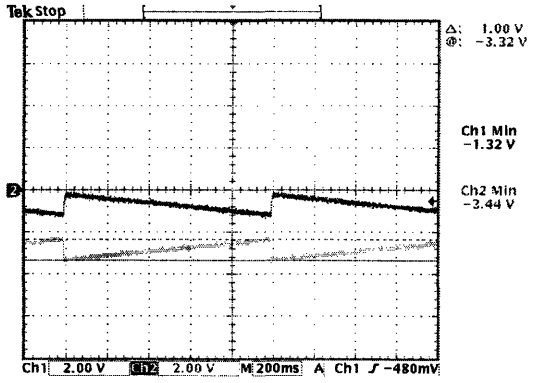

Figure 5-13: Output of subtractor with a 1-V sawtooth wave input

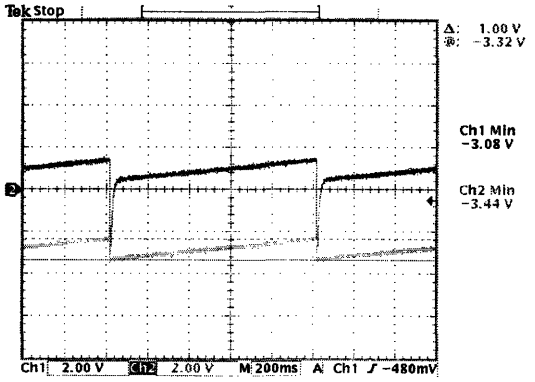

Figure 5-14: Output of lead compensator with a 1-V sawtooth wave input

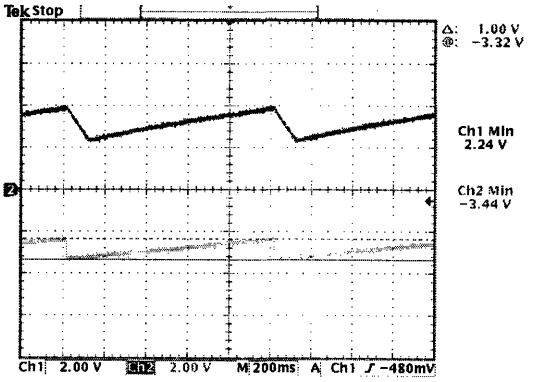

Figure 5-15: Output of square-rooter with a 1-V sawtooth wave input

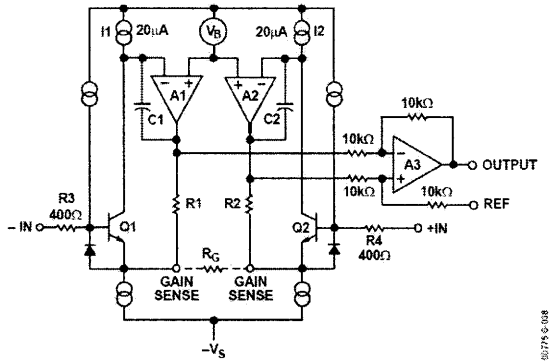

Figure 5-16: Simplified schematic of the AD620 instrumentation amplifier

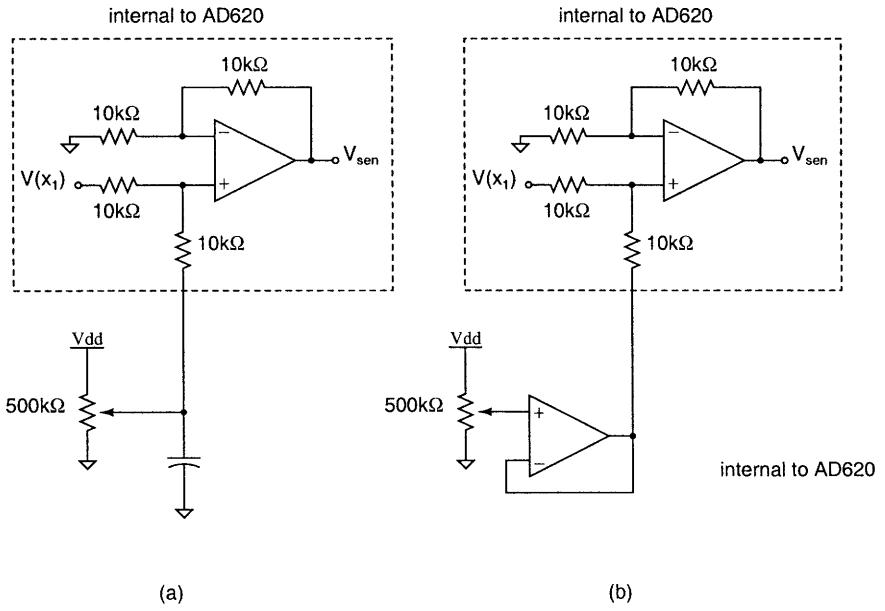

Figure 5-17: Biasing fix for the position sensor

Appendix A

Schematics

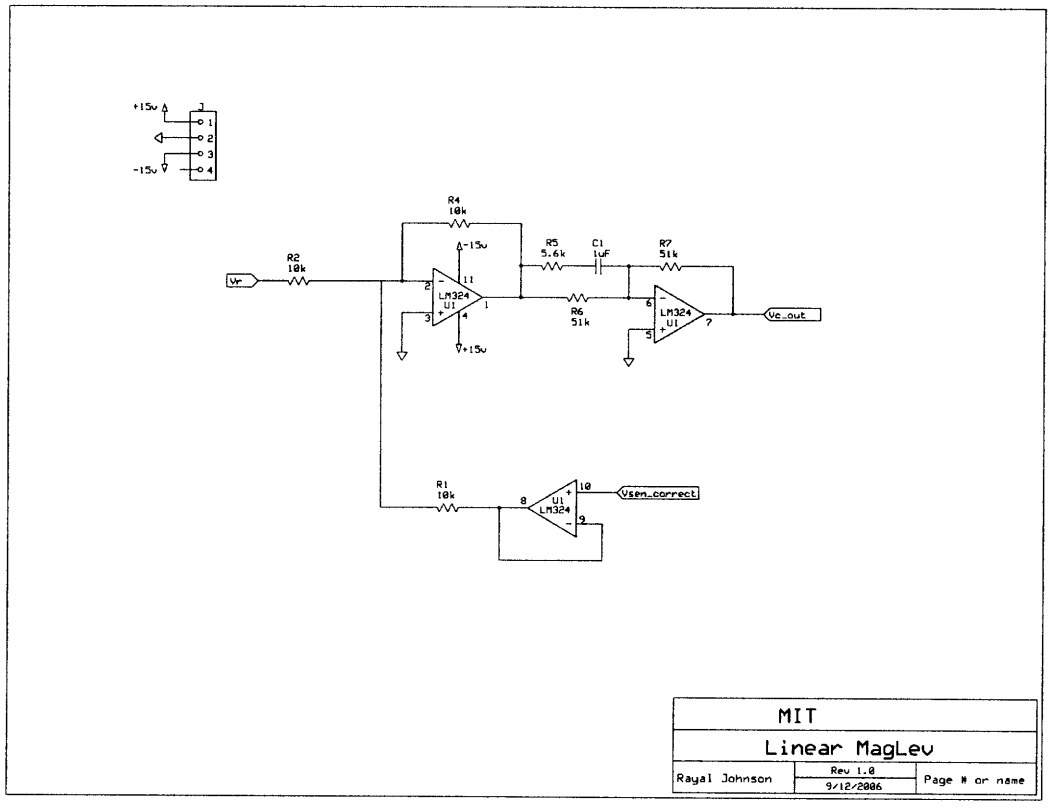

Figure A-1: Subtractor and lead compensator

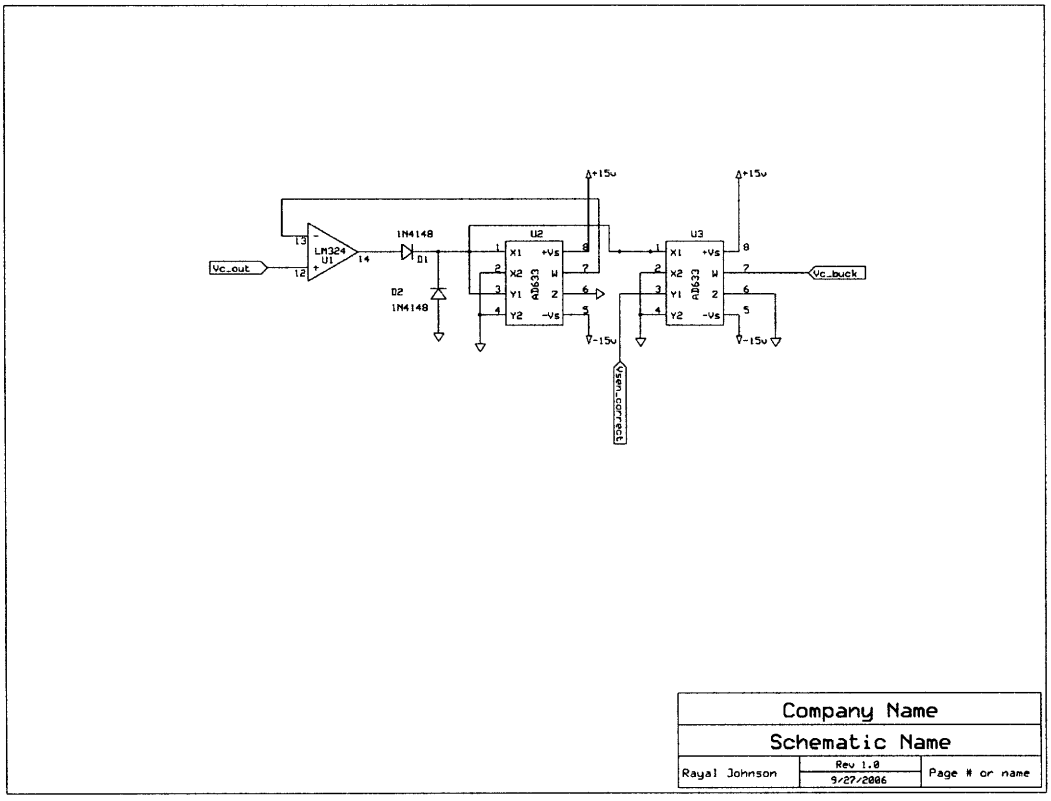

Figure A-2: Nonlinear compensator

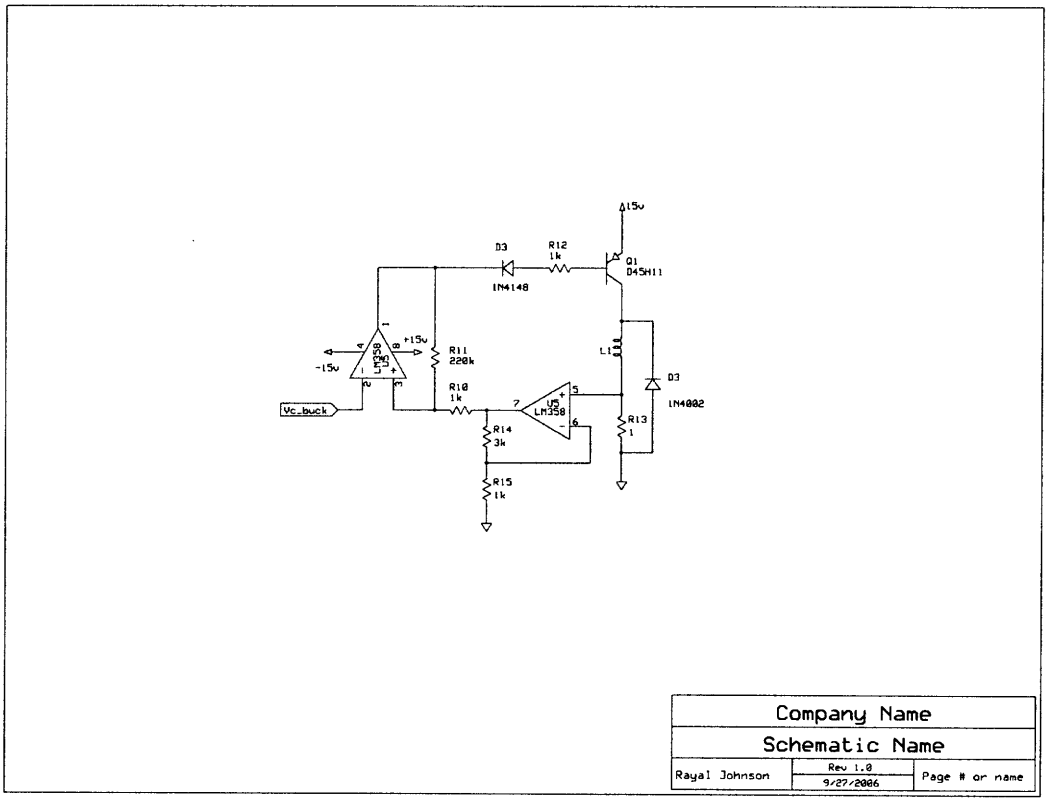

Figure A-3: Current driver

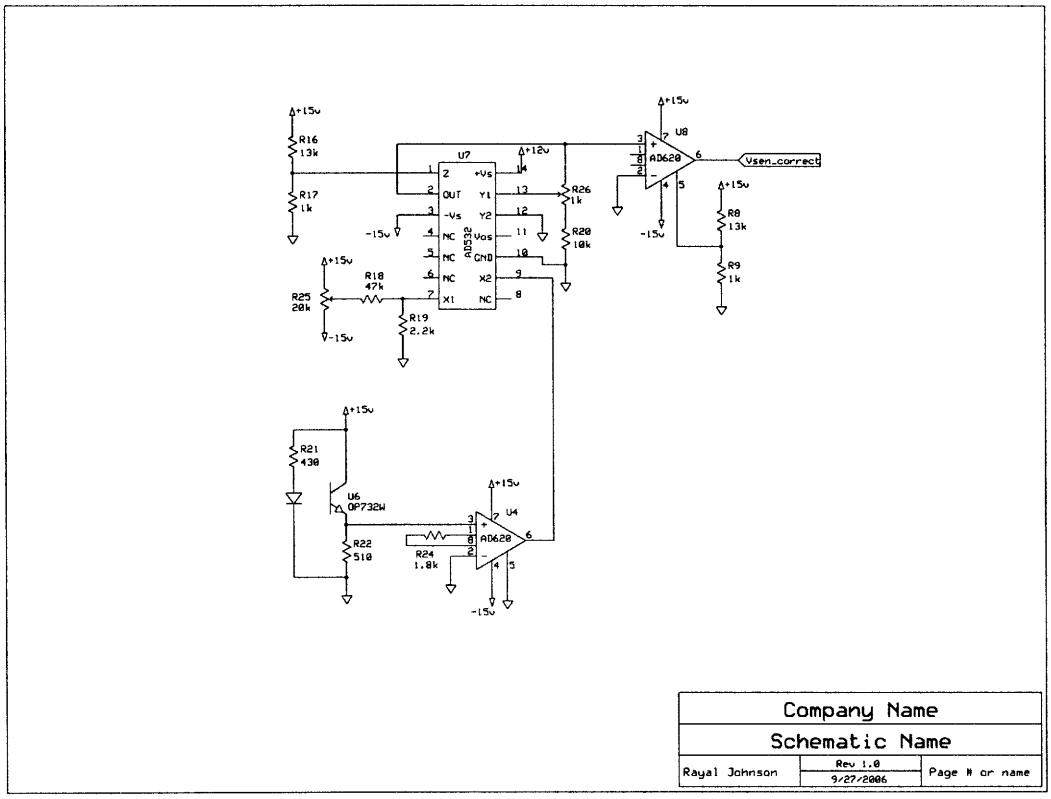

Figure A-4: Position sensor circuit

Bibliography

[1] I. Dancy. Educational hardware for feedback systems. Master of engineering in electrical engineering and computer science, Massachusetts Institute of Technology, September 2004.

[2] Rick Hoadley. Home-built magnetic levitator. web, April 2006. Date is date accessed.

[3] W.G. Hurley, M. Hynes, and W.H. Wölfle. Pwm control of a magnetic suspension system. *IEEE TRANSACTIONS ON EDUCATION*, 47(2):165–173, 2004.

[4] John G. Kassakian, Martin F. Schlect, and George C. Verghese. *Principles of Power Electronics.* Addison-Wesley Publishing Company, Inc., 1991.

[5] Philip Krein. *Elements of Power Electronics.* Oxford University Press, Inc, 1998.

[6] K. Lundberg. Become one with the transistor for solid-state circuits. February 2006.

[7] J.K. Roberge. *Operational Amplifiers: Theory and Practice.* John Wiley and Sons, 1975.

[8] J-J.E. Slotine and W. Li. *Applied Nonlinear Control.* Prentice-Hall, Inc, 1991.

[9] Feedback Systems. Lab 2 maglev project. web, November 2005.

[10] OPTEK Technology. Long distance reflective switch. Datasheet.

[11] D.L. Trumper. *Magnetic Suspension Techniques for Precision Motion Control.* PhD thesis, Massachusetts Institute of Technology, 1990.

[12] Y. Tsividis. Externally linear, time-invariant systems and their application to companding signal processors. *IEEE Trans. on Circuits and Systems–II*, pages 65–85, February 1997.

[13] B.D. Wedlock and W.G. Hurley. Correction to "pwm control of a magnetic suspension system". *IEEE TRANSACTIONS ON EDUCATION*, 47(4):508, 2004.

[14] David Williams. Electromagnetic levitator. *Electronics Now*, pages 33–34,67–70, February 1996.

[15] H.H. Woodson and J.R. Melcher. *Electromechanical Dynamics - Part-I.* John Wiley and Sons, 1968.